Nitric Oxide Releasing Titanium Surfaces for Antimicrobial Bone-Integrating Orthopedic Implants

Man Li,[†] Jenny Aveyard, [†] George Fleming, [†] Judith M. Curran, [†] Fiona McBride,[‡] Rasmita Raval[‡] and Raechelle A. D'Sa[,†]*

[†] School of Engineering, University of Liverpool, L69 3GH, UK.

[‡] The Open Innovation Hub for Antimicrobial Surfaces, Surface Science Research Centre, Department of Chemistry, University of Liverpool, L69 3BX, UK

ABSTRACT: Titanium implants in orthopedic applications can fail due to infection and impaired integration into the host. Most research efforts that facilitate osseointegration of the implant have not considered infection and vice versa. Moreover, most infection control measures involve the use of conventional antibiotics which contributes to the global epidemic of antimicrobial resistance. Nitric oxide (NO) is a promising alternative to antibiotics and whilst researchers have investigated NO releasing coatings, few reports on the function/robustness or the mechanism of NO release. Our comprehensive mechanistic study has allowed us to design, characterize and optimize NO releasing coatings to achieve maximum antimicrobial efficacy towards bacteria with minimum cytotoxicity to human primary osteoblasts *in vitro*. As the antibiotic era is coming to an end and the future of infection control

continues to demand new alternatives, the coatings described herein represent a promising therapeutic strategy for use in orthopedic surgeries.

KEYWORDS: nitric oxide; diazeniumdiolates; primary amine; orthopedic implants; biofilm inhibition

1. INTRODUCTION

Orthopedic implants made from titanium are used extensively given their excellent mechanical properties, corrosion resistance and lack of allergenic or immunogenic response.[1-3] However, there are two major causes of implant failure: infections and poor tissue integration. The reported rates of these failures differ based on the study, with approximately 20% due to infection and 18% due to poor integration.[4-5] Much research in this field has focused on developing coatings to prevent bacterial colonization while ignoring integration of the implant or vice versa, promoting osseointegration, while ignoring the infection issue. To achieve longevity of the implants, both of these modalities must be considered simultaneously.

Implant-associated infections represent a serious complication as once bacteria colonize the surface, they form biofilms, which are more difficult to treat, requiring up to a 1000-fold increase in the antimicrobial dose.[6-7] Once an infection takes place on a titanium implant, repeated revision surgeries are often required and can lead to poor implant integration, bone loss and soft tissue defects.[8-9] Orthopedic implant infections are caused most often caused by *Staphylococcus species* (*S. aureus* and *S. epidermidis*) or *Pseudomonas aeruginosa* which can be acquired during surgery or subsequently through a hematogenous route.[10-11] Moreover, implants that are transmucosal and percutaneous (e.g. dental and external fixation pins) are

more susceptible to infection as opportunistic bacteria that reside on the skin mucosa can colonize the peri-implant soft tissue which can lead to a peri-implant bone infection.[12-13] Localized delivery of antibiotics via a coating layer on the implant is seen as a promising strategy to prevent infections and subsequent failure of the implant. However, given the rise in the global epidemic of antimicrobial resistance, much focus has changed to the development of alternative antimicrobials such as silver [14-15] zinc ions,14 bioactive antibodies,[16] antimicrobial peptides[17-18] and nitric oxide[19-20] which have a low tendency to developing multi drug resistant bacteria.

Nitric oxide (NO) is a potent broad spectrum antimicrobial and part of the body's defense mechanism that is activated by inflammatory cells (neutrophils and macrophages) which are responding to invading pathogens such as bacteria, protozoa and fungi.[21-22] The antimicrobial activity of NO is attributed to the reactive nitrogen oxide species (RNOS) that are produced through the spontaneous reaction of NO with oxygen or superoxide that cause damage to bacterial DNA, proteins and lipid membranes.[23-24] The formation of these RNOS become significant or antimicrobial when the concentration of NO is >1μM.[23] Given that there are several mechanistic pathways for NO to inactivate bacteria, studies have shown that there is a low tendency for bacteria to develop resistance to this antimicrobial.[25-26] Furthermore as eukaryotic cells have evolved mechanisms that are capable of scavenging these RNOS, it is thought that NO will exhibit a low toxicity on the host.[21]

Although NO is clearly identified as a potent antimicrobial, its clinical utility is challenging as NO is a highly reactive gas with a short half-life[27]. As such, there has been much research focused on the development of NO donors such as *N*-diazeniumdiolates, *S*-nitrosothiols, organic nitrates, metal nitrosyls which can store and release NO for more prolonged periods of time under requisite conditions.[28-30] The most commonly reported *N*-diazeniumdiolates

(containing the [N(O-)N=O]) are adducts formed from a NO dimer with a secondary amine nucleophile.[27, 29] These *N*-diazeniumdiolates can spontaneously decompose with tunable half-lives dependent on the structure of the nucleophile (amine), pH and temperature.[29] As secondary amine diazeniumdiolates are formed much easier, much work has focused on these rather than primary amine diazeniumdiolates.[31-34] Although many of these studies have investigated how NO can be released for biomaterial/medical device applications, there is a paucity of information regarding the mechanism of release and the robustness of the coatings. For example, Ho and coworkers focused on the feasibility of using plasma polymerization to coat polymer surfaces with allylamine and diallylamine coatings, followed by the incorporation of diazeniumdiolates.[34] In this study, although they have looked at primary and secondary diazeniumdiolates and have obtained a higher NO payload with the secondary diazeniumdiolate,[34] they have not evaluated the stability or shelf-life of the coatings or investigated the potential cytotoxicity of the materials. Moreover, the underlying coatings are not optimized to promote osseointegration.

In previous work, Curran *et al* have established that amino terminated silanes (as opposed to methyl, hydroxyl, or thiol) can control cell responses, resulting in the formation of high quality de novo tissue.[35-36] These comprehensive investigations were performed with a variety of silanized glass surfaces to understand the effect of silane chain length on associated osteoinductive properties of the surface.[35] Within this work, only the longer chain silanes containing pendant amino groups resulted in the formation of an apatite-like layer on the surface that induced a significantly enhanced osteoinductive response across the entirety of the surface.

Based on the work of Curran and coworkers, we have chosen the amino-terminated silane (11-Aminoundecyltriethoxysilane, AUTES) with the most consistent and homogeneous

osteoinductive property and used this to tether NO. The hypothesis here is as the underlying surface is known to be osteoinductive, once the NO is released and any potential infection during implantation is averted, osseointegration can take place. Within this preliminary study we investigate the effect of NO on the initial and prolonged (after 7 days) viable adhesion of primary human osteoblasts to the modified surfaces. However, since primary diazeniumdiolates are not as well studied and do not release as much NO[37], we wanted to test another potentially osseointegrative promoting silane containing a secondary amine in order to investigate the effects of primary vs secondary amines in terms of antimicrobial efficacy.

In this study, we report on the functionalization of Ti with two different aminosilanes and the subsequent tethering of diazeniumdiolates onto the silanes. We have carried out a comprehensive mechanistic study of NO releasing coatings developed to understand the kinetics and payload of release as a function of the stability of the silane, the nature of the amino functional group and pH of release. This mechanistic understanding will allow fine tuning of the antimicrobial efficacy to prevent infection at 6 hrs (time frame for initial bacterial adhesion vs. mammalian cell adhesion) in the so called "race to the surface". The antimicrobial efficacy against *Staphylococcus aureus* and *Pseudomonas aeruginosa* have been studied at 6 and 24 hrs and cytocompatibility of the surfaces with primary human osteoblast cells was investigated in order to improve the integration of implants with bone.

2. MATERIALS AND METHODS

2.1 Experimental Materials. Ti rods (ø 6.4mm, 99.7% metal basis) were purchased from Alfa Aesar and cut into pieces 1.5 mm in thickness. 6-Aminohexyl-3-aminopropyl trimethoxysilane (AHAP3, 95%), 11-Aminoundecyltriethoxysilane (AUTES, > 95%), n-

Decyltrimethoxysilane (DTMS, 97%) were purchased from Fluoro Chem. Ethanol, acetic acid (HAc), sodium acetate (NaAc), Luria Bertani Broth (LB Broth), LB agar, Dulbecco's Modified Eagle Medium (DMEM), fetal bovine serum (FBS), Penicillin-Streptomycin, Trypsin-EDTA solution, formaldehyde solution and Triton™ X-100 were purchased from Sigma-Aldrich. 4′,6-diamidino-2-phenylindole (DAPI) staining mounting gel and ActinGreen ™ 488 reagent kit were obtained from Thermo Fisher Scientific.

2.2 Titanium Pre-Treatment. Ti discs were polished with SiC sand paper (1200-grit) and then washed with ethanol and DI water for 15 mins each. Washed Ti discs were then air dried at room temperature and stored in a desiccator until use.

2.3 Silanization and Diazeniumdiolate-Functionalization. Pristine polished Ti discs were immersed in 10 wt % silane solutions (Amino-silanes: AHAP3, AUTES and Control alkyl silane: DTMS) prepared in ethanol and shaken on a gyro-rocker (SSL3, Stuart) at 70 rpm for 4 hrs. Samples were then washed with ethanol 3 times to remove unreacted silane and cured in an oven at 80° C for 4 hrs. At the end of this time, samples were then stored in a desiccator until diazeniumdiolate functionalization. Silanized samples are referred to as AHAP3, AUTES and DTMS, respectively. Silanized Ti discs were functionalized with diazeniumdiolates in an in-house built stainless steel NO reactor as previously reported.[38] Briefly, the reactor chamber was purged with 6 bar argon (BOC, Guildford, UK) for 5 mins (3 x) and 10 mins (3 x) to remove atmospheric oxygen and water. Then nitric oxide (NO) (BOC, Guildford, UK) was introduced into the reactor at 5 bar for 3 days. At the end of this time, residual NO was removed by flushing the chamber with 6 bar argon for 5 mins (2 x) and 10 mins (2 x). Diazeniumdiolate functionalized Ti samples were then stored at -20°C until use. Diazeniumdiolate functionalized samples are referred to as Ti/NO, AHAP3/NO, AUTES/NO and DTMS/NO, respectively. It should be noted that Titanium samples will have

an oxide layer on the surface and most likely exist as TiOx. Moreover as Ti and DTMS do not possess any amine functionality, there is no possibility of forming *N*-diazeniumdiolates, and as such these are control samples. The nomenclature is kept as Ti/NO and DTMS/NO for consistency and ease of readership.

2.4 Characterization. *2.4.1 Contact Angle Analysis.* Static contact angles (Attension ThetaLite, Biolin Scientific, Västra Frölunda, Sweden) were used to determine the changes in surface wettability of all samples. The sessile drop method was used and contact angle measurement images were taken using OneAttension software (Biolin Scientific, Västra Frölunda, Sweden). Three random spots were performed per sample type (n=3) and mean values ± standard deviations of the samples were recorded and repeated twice.

2.4.2 Atomic Force Microscopy Analysis. Atomic force microscopy (AFM) was used to observe the surface topography changes of silanized samples (Bruker Multimode 8 fitted with a NanoScope V controller; Bruker, Billerica, MA, USA). Samples were imaged in air in ScanAsyst mode using a silicon RTESPA-525 tip, operating at a scan rate of 0.9 Hz. At least three replicate regions including the centre and edge of 10 x 10 μm^2 of each sample were imaged and repeated twice. The mean roughness (R_a) and root mean square roughness (R_q) were measured using NanoScope Analysis 1.7 software.

2.4.3 X-ray Photoelectron Spectroscopy. Functionalized surfaces were analyzed by X-ray photoelectron spectroscopy (XPS) on an Axis-Supra instrument from Kratos Analytical with monochromatic Al Kα radiation (225W). Survey scan spectra were recorded at a pass energy of 160 eV and a 1 eV step size. High resolution scans were acquired at a pass energy of 20 eV and a 0.1 eV step size. The XPS spectra were recorded in normal emission. Three random areas on each sample were analyzed and the results are reported as the mean average atomic percentage concentration (at. %) ± standard deviations. Spectra were processed using

CasaXPS 2.3.19PR1.0 software (Casa software, UK) and charge calibrated to C 1s at 284.8 eV. Spectra were curve fitted with a mixed Gaussian-Lorentzian function after Shirley background subtraction.

2.4.4 NO Release Measurement. Nitric oxide release from samples was measured using a Sievers 280i Chemiluminescence Nitric Oxide Analyzer (NOA280i, GE, USA). The instrument measures nitric oxide based on a gas-phase chemiluminescent reaction between nitric oxide and ozone:

$NO + O_3 \rightarrow NO_2^* + O_2$

$NO_2^* \rightarrow NO_2 + h\nu$

Emission from electronically excited nitrogen dioxide is in the red and near-infrared region of the spectrum, and is detected by a thermoelectrically cooled, red-sensitive photomultiplier tube. Before measurement, calibration was carried out by using zero air filter and 89.2 ppm NO (g) (balance nitrogen). The diazeniumdiolate functionalized samples (6.4 mm diameter, 1.5 mm thick) were immersed in 5 ml of acetic acid buffer (pH 4) or phosphate buffered saline (PBS; pH 7.4 and pH 8.5) at room temperature in a three-neck round bottom flask. Nitrogen gas was continuously sparged though the buffer at a flow rate of 70 mL / min measured with a gas flow meter. An additional nitrogen flow of 130 mL / min passed through the headspace of the vessel to the bubbled solution phase, according to the NOA manual. While the standard NOA restrictor provides a flow rate of 150 ml / min. A vacuum pump connected with the NOA is used to draw the mixed gases in to the reaction cell and maintains the pressure of the reaction cell. Nitric oxide release was measured at an interval of 1 s over more than 20 hrs. Each sample was measured in triplicate.

2.5 Biofilm Assay and Morphology Analysis. *Staphylococcus aureus* (*S. aureus*) ATCC 25923 and *Pseudomonas aeruginosa* (*P. aeruginosa*) PA01 were used to evaluate the biofilm inhibition efficiency of the nitric oxide releasing surfaces. Overnight cultured bacteria were diluted to 10^6 CFU/mL according to McFarland Standards in LB broth. Samples were placed in a 48 well-plate and 500 µL diluted bacterial solution was added to each well before incubating at 37 °C to allow biofilm formation. After incubation, samples were gently washed with PBS once to remove any unattached planktonic bacteria and then 1 mL of fresh LB broth was used to remove and re-suspend the biofilms. The bacterial CFU was determined after serial dilution of the bacterial suspension using the Miles and Misra method on LB agar plates.[39]

After incubation with bacteria, the samples were fixed with 2.5% glutaraldehyde solution in sterile PBS for 4 hrs at 4 °C, then dehydrated with increasing concentrations of ethanol (30, 50, 75, 90, 95, and 100 v/v %) for 10 min. After drying the samples were coated with gold (Q150T ES sputter coater; Quorum, East Sussex, UK) before SEM imaging (JSM 7001F FEGSEM; JEOL, Tokyo, Japan).

2.6 *In Vitro* Cell Culture and Immunocytochemistry Analysis. Primary human osteoblast cells were expanded and maintained *in vitro* in DMEM media supplemented with 10% FBS and 1% penicillin-streptomycin in a humidified atmosphere of 5% CO_2 at 37 °C and used between passages 5 and 10. Upon confluence cells were rinsed in sterile PBS and incubated with trypsin-EDTA for 3 minutes at 37 °C to remove the cells from tissue culture polystyrene (TCPS) and retain in solution, diluted to 1 x 10^5 cells/ml using the afore mentioned culture medium. Samples were incubated with 1 ml of cell suspension per well in 24-well culture plates. The media was replaced with fresh cell culture media every 3 days.

At day 7 of culture, cells were prepared for staining using the following protocols. Medium was removed from the wells and samples were rinsed with sterile PBS for 5 minutes at 37 °C. Cells were then fixed using 4% formaldehyde for 15 min at room temperature, followed by rinsing with PBS. Then cells were permeabilized with 0.5% Triton® X-100 for a further 15 min at room temperature. After washing 3 times with PBS, cells were incubated with diluted Oregon Green PhallodinTM 488 kit (5µg/ml) for 30 min at 4°C followed by further rinsing with PBS prior to mounting with DAPI staining mounting medium (Vector, UK). Cell morphology images were obtained by confocal laser scanning microscopy (LSM 510, Zeiss, Germany). 6 images were taken per samples and representative images are shown. Images were processed using ImageJ 1.48 software.

2.7 Statistical Analysis. One-way analysis of variance (ANOVA) was used to analyze the differences among various treatment samples. The Student-Newman-Keuls (SNK) method was carried out to determine significance between treatment types. A value of $p < 0.05$ was taken as being statistically significant.

3. RESULTS AND DISCUSSION

3.1 Synthesis of *N*-Diazeniumdiolate-Functionalized Titanium. The diazeniumdiolate functionalized Ti surfaces were synthesized via a two-step method illustrated in Figure 1. Polished Ti surfaces were functionalized with silanes with or without primary and secondary amines; 6-Aminohexyl-3-aminopropyl trimethoxysilane (AHAP3): 1 primary amine and 1 secondary amine, 11-Aminoundecyltriethoxysilane (AUTES): 1 primary amine and n-Decyltrimethoxysilane (DTMS): no amine. The silane-modified Ti substrates were then exposed to high pressures of NO (5 bar) over 72 hrs to allow formation of diazeniumdiolate NO donors.

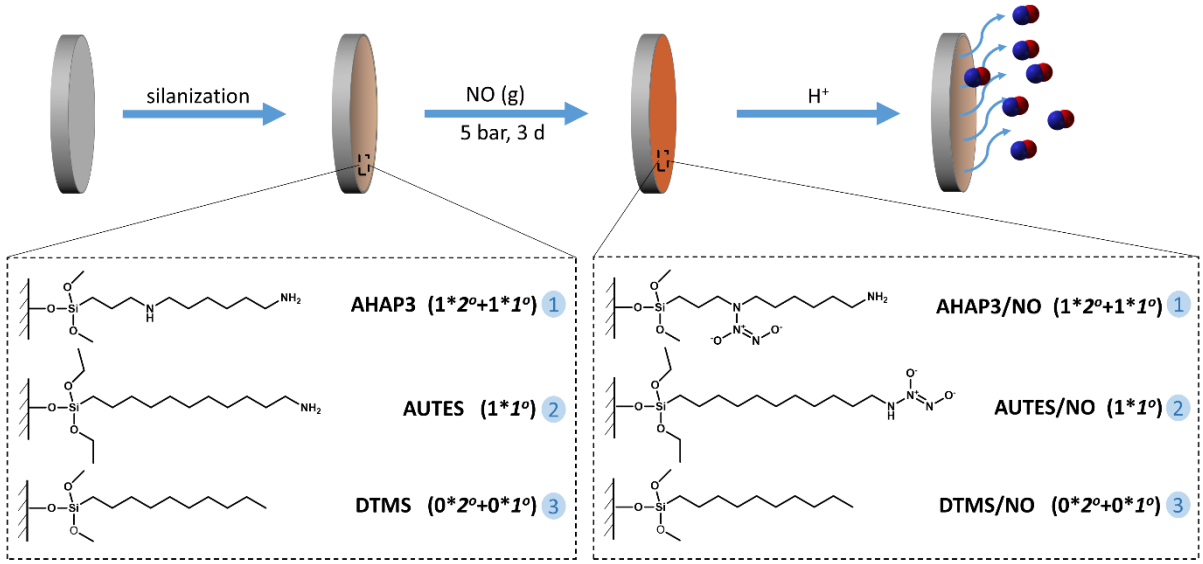

Figure 1. Diazeniumdiolate functionalization of titanium surfaces.

3.2 Surface Wettability: Static Water Contact Angle. The wettability of the Ti substrates before and after functionalization was determined using static contact angles with the results shown in Figure 2. Pristine Ti had an average contact angle of 64°. After silanization, the contact angles for AHAP3, AUTES and DTMS films on Ti increased to 78, 83 and 101°, respectively. The increase in contact angle can be attributed to the presence of hydrophobic alkyl silane chains confirming functionalization of the surface. DTMS displayed the most hydrophobic character, as there is no electronegative amino group present in the silane molecule.

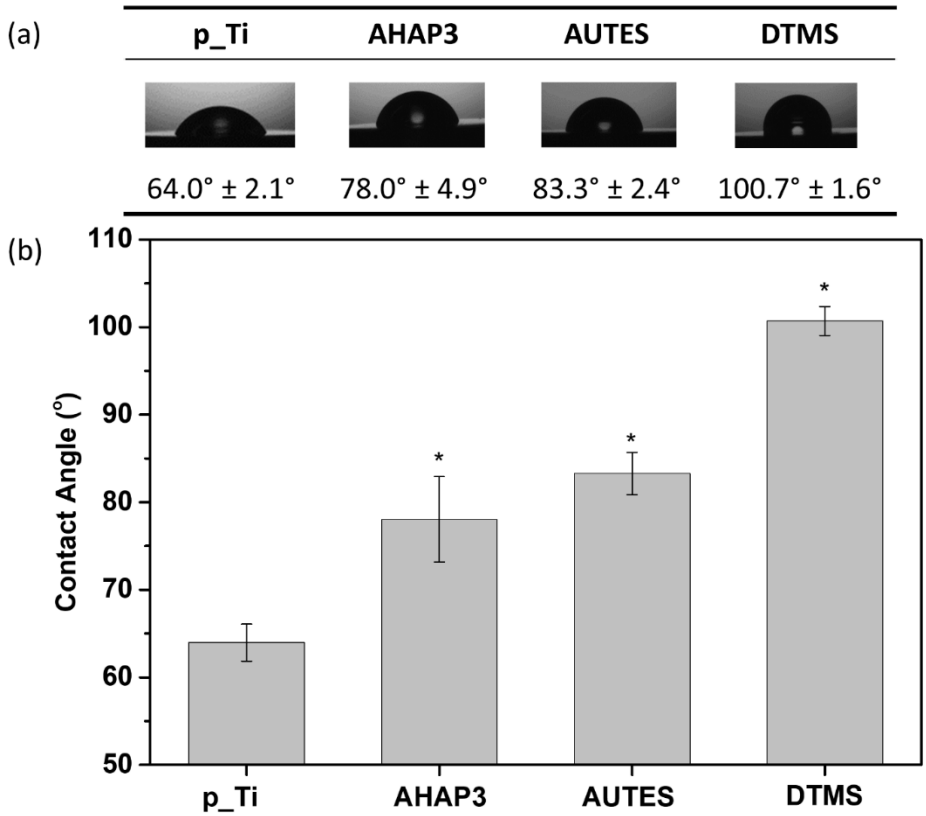

Figure 2. Measurement of contact angle with water drops at room temperature. a) Contact angle images of pristine Ti (p_Ti) and silanized p_Ti with AHAP3, AUTES and DTMS. b) Measurement of contact angles of p_Ti and silanized p_Ti. Each bar represents mean ± SD (n=3). *$p < 0.05$, relative to the control.

3.3 Surface Topography: Atomic Force Microscopy. The topography of Ti and functionalized Ti surfaces was investigated using AFM (Table 1 and Figure 3). Pristine Ti has a roughness of 35.5 ± 0.8 nm (R_a) (Figure 3a) and all of the silanized surfaces showed a statistically significant increase in roughness (Figure 3b- d). This is indicative of the deposition of multiple layers of silane on the surface. Indeed there is visible aggregation of the silane observed on all of the silanized surfaces (Figure 3b-d). The silanized surfaces displayed roughness values (R_a) of: AHAP3 (108.1 ± 16.4 nm), AUTES (87.1 ± 8.7 nm) and DTMS (64.8 ± 17.4 nm) (also listed in Table 1.).

Table 1. Topography of Silanized Surfaces

roughness	p_Ti	AHAP3	AUTES	DTMS
***R*q (nm)**	46.4 ± 2.1	135.0 ± 26.0 [a]	109.2 ± 9.1 [a]	80.9 ± 22.0
***R*a (nm)**	35.5 ± 0.8	108.1 ± 16.4 [a]	87.1 ± 8.7 [a]	64.8 ± 17.4 [a]

[a] indicates statistical significance ($p < 0.05$) between the control and silanization surfaces.

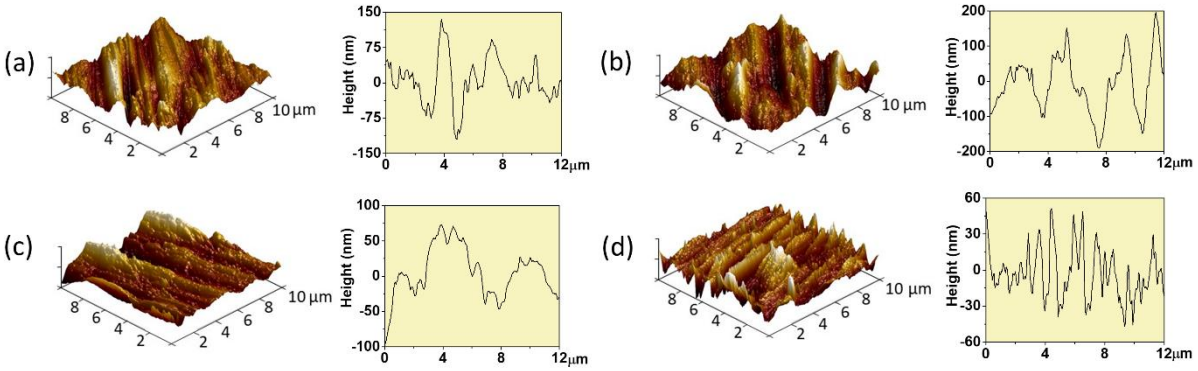

Figure 3. AFM height mode of silanized surfaces. The cross-sections of 10 × 10 µm^2 size images are shown at different z-axis maximum heights. a) p_Ti, b) AHAP3, c) AUTES, d) DTMS.

3.4 Surface Chemistry: X-ray Photoelectron Spectroscopy. The surface chemistry of the silanized surfaces pre- and post- diazeniumdiolate treatment were analyzed by XPS with the resultant at. % shown in Table 2. XPS analysis shows that pristine Ti consists of Ti, C, O and N. After silanization with all 3 silanes, the Ti 2p peak decreases with an increase in the C 1s peak and introduction of the Si 2p peak, confirming the silanization of the surface. Following exposure of the silanized Ti surfaces to NO, the at. % of the C 1s peak decreases with a concomitant rise in the O 1s and N 1s peaks confirming formation of the *N*-diazeniumdiolate functional group.

Table 2. Atomic Surface Concentration (at. %) of Pristine Ti Surface, Silanized Surfaces and Diazeniumdiolates-Functionalized Surfaces

sample	C (1s)	O (1s)	N (1s)	Ti (2p)	Si (2p)
p_Ti	28.2±1.4	52.2±0.8	0.6±0.5	18.9±1.1	-
AHAP3	63.9±5.3	15.2±5.4	9.6±1.4	1.3±2.3	9.9±1.2
AUTES	75.0±0.3	11.5±0.2	3.7±0.4	-	9.8±0.2
DTMS	47.9±0.8	34.4±0.5	1.7±0.3	11.7±0.5	4.2±0.3
Ti/NO	49.3±2.7	39.4±2.2	1.7±0.8	9.5±1.3	-
AHAP3/NO	57.1±1.2	26.4±1.1	10.3±0.3	0.6±0.5	5.5±0.2
AUTES/NO	71.5±0.2	17.8±0.2	1.8±0.5	0.1±0.1	8.8±0.4
DTMS/NO	62.2±3.5	25.8±4.9	0.8±0.4	4.1±2.0	7.0±1.4

The silanization and functionalization with diazeniumdiolate can also be corroborated by analyzing the curve fitted high resolution N 1s spectra shown in Figure 4 (with the associated quantitative information given in Table S1 of the Supplementary Information). The presence of nitrogen on pristine Ti (Figure 4a) is due to the nitrogen contamination of the raw material (N: 0.02% in Ti rod, data from certificate of analysis document, Alfa Aesar). Following silanization with the aminosilanes, AHAP3 and AUTES, two additional states of nitrogen observed, with binding energies at ~400.5 eV (N-H) and ~401.6 eV (N+) (Figure 4c and 4e). After exposure to high pressures of NO, diazeniumdiolate formation was confirmed via the presence of the new peaks observed, indicative of N-H (400.5 eV), N-O (402.3 eV), and NO_4^- (~407 eV) bonds. Moreover, the presence of the N-O bond is observed with a decrease in the N-H bond, confirming the nucleophilic attack of the amine group on the NO dimer forming the diazeniumdiolate functional group. Interestingly, DTMS does not have any pendant amino groups but after exposure to NO gas, the N 1s envelope shows the presence of N-O

peak (28%). This is probably due to some physisorbed NO on the surfaces that have been converted to nitrates and nitrites.

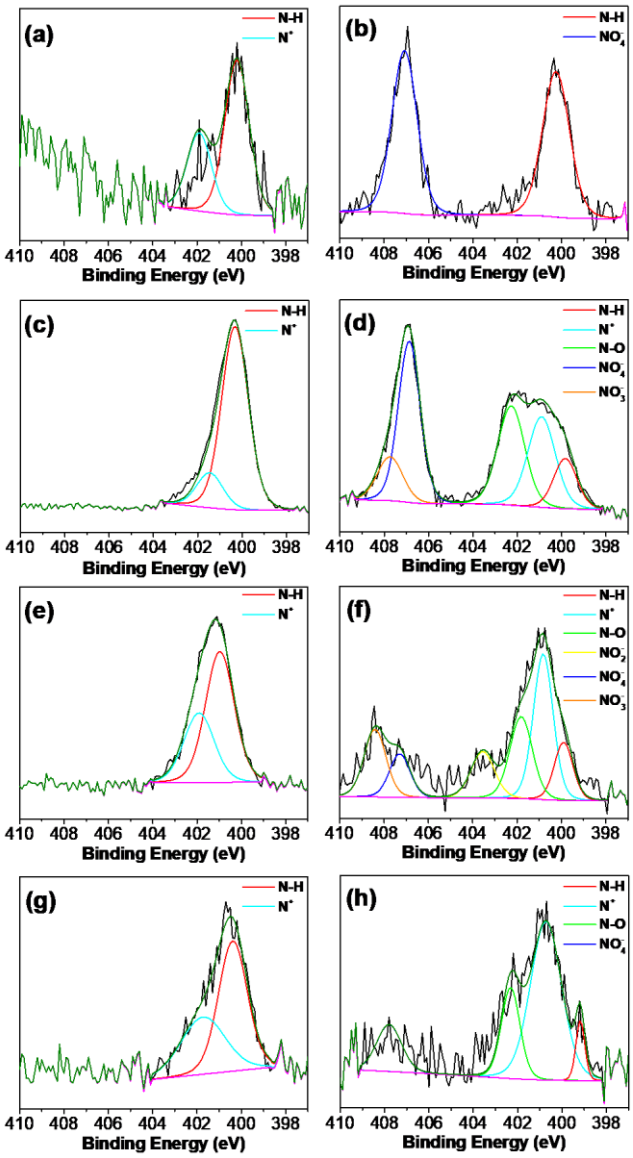

Figure 4. High-resolution N 1s spectra of (a) p_Ti, (b) Ti/NO, (c) AHAP3, (d) AHAP3/NO, (e) AUTES, (f) AUTES/NO, (g) DTMS and (h) DTMS/NO. The peak at ~401.6 eV represent $–N^+$ and the N-O bond shows a bonding energy at ~402.3 eV, shows successful formation of diazeniumdiolates.

3.5 NO Release from Diazeniumdiolate-Functionalized Surfaces. In order to understand the effects of pH on NO release, the NO-payload from the diazeniumdiolate-modified surfaces was determined using a chemiluminescence nitric oxide analyzer in acetate and PBS buffers at pH 4, 7.4 and 8.5. The NO release profiles of Ti/NO, Ti-AHAP3/NO, Ti-AUTES/NO and Ti-DTMS/NO are shown in Figure 5. The total concentration of NO after 1 hr (t[NO]), half-life of NO release ($t_{1/2}$), maximum instantaneous NO release concentration ($[NO]_m$), time required to reach $[NO]_m$ (t_m) and NO release duration (t_d) from each surface were determined and the values are summarized in Table 3. The NO payload and release kinetics were dependent upon the number and class of amines in the silane, the pH of the release buffer and if a monolayer or multilayer of silane was present on the surface.

AHAP3/NO: At pH 4, AHAP3/NO surfaces released NO at a maximum instantaneous NO release concentration of 1.8 $\mu M \cdot s^{-1}$ with 1005.4 μM NO being released in a burst during the first hour. At pH 7.4, the concentration of NO released was less than that observed at pH 4, with 676.8 μM of NO released during the first hour. At pH 8.5, the AHAP3/NO surface released a NO concentration of 330.5 μM during the first hour.

AUTES/NO: At pH 4, AUTES/NO surfaces released a maximum instantaneous NO release concentration of 5.6 $\mu M \cdot s^{-1}$ and 1883.6 μM NO was released in a burst during the first hour. At pH 7.4, the concentration of NO released was less than that observed at pH 4. 476.2 μM of NO was released during the first hour. At pH 8.5, the AUTES/NO surface released 133.7 μM during the first hour.

DTMS/NO: At pH 4, DTMS/NO surface, released 231.1 μM of NO with a maximum instantaneous NO release concentration of 0.4 $\mu M \cdot s^{-1}$. At pH 7.4, the concentration of NO released was less than that observed at pH 4. The final concentration of NO released was 26

μM during the first hour. At pH 8.5, the DTMS/NO surface released no measurable NO. DTMS/NO has no amine in its backbone and therefore cannot form an *N*-diazeniumdiolate.

3.6 Mechanism of NO Release. The mechanism of NO release is dependent on three factors as described below: pKa of the amine, class of amine (primary vs secondary) and quality of the silane layer formed on the surface.

pKa: The NO release from diazeniumdiolate occurs via protonation of the amine precursor and the release kinetics are dependent upon the pKa of the amine. As such, the higher the pKa the easier the protonation and the faster the release at physiological conditions. The rate of release of NO can also be increased by other factors such as the presence of neighboring amines which can act as a proton source[40] and an increase in temperature.[41] This is indeed what was experimentally observed for the AHAP3/NO and the AUTES/NO surfaces; at pH 4 these surfaces showed a burst release of NO.

Class of amine: Keefer and co-workers have demonstrated that primary amine diazeniumdiolates decompose to HNO and NO with the product ratio dependent on the pH and the basicity of the nitroso oxygen formed.[33] In contrast, secondary amines only undergo decomposition based on pH mediated protonation to produce exclusively NO.[33] Keefer has shown that primary amine diazeniumdiolates decompose: (a) exclusively to NO at pH 5; (b) to a mixture of HNO and NO at pH 5-8, and (c) exclusively to HNO above pH 8. In our work, AHAP3/NO has the potential to form one secondary and one primary amine diazeniumdiolate and AUTES/NO has the potential to form only a primary amine diazeniumdiolate. Therefore, based on Keefer's mechanism,[33] AHAP3/NO and AUTES/NO will release the highest concentration of NO at pH 4 as both the primary and secondary amines exclusively decompose to NO. The concentration of NO will then decrease as the pH of the release buffer increases due to the presence of primary amines and subsequent

decomposition to HNO. Despite the AHAP3 releasing lower amounts of NO at pH 4 (1005.4 μM) than the AUTES (1883 μM), the release concentration exceeds the concentration released by AUTES at pH 7.4 due to the presence of a secondary amine in AHAP3.

Number of amines/Quality of silane layer: AHAP3 has one secondary amine and one primary amine and therefore the potential to form of two diazeniumdiolates and have double the payload of NO at pH 4. In solution, this is indeed what is observed, where AHAP3/NO (10 μl/5 ml PBS) shows a maximum NO release of 1993.3 $\mu M \cdot s^{-1}$, in comparison with AUTES (Figure S1). However, we observed the opposite when the silanes were immobilized on the surface, with AHAP3/NO and AUTES/NO having NO payloads of 1005.4 μM and 1883.6 μM within the first hour. The lower payload observed here is due to the quality of the silane monolayer formed.

A more cohesive silane coverage on Ti surfaces should yield a higher NO payload. AUTES forms a monolayer on the surface through hydrolysis of an ethoxy leaving group to generate silanol containing species that readily condenses on the surface. The faster the hydrolysis of the silane, the faster the condensation and the increase in the self-condensation/aggregation reactions (a less cohesive monolayer is formed on the surface). The rate of hydrolysis of the alkoxy groups are dependent on their size ($CH_3O > C_2H_5O > t\text{-}C_4H_9O$), meaning that a methoxysilane hydrolyses 6 - 10x quicker than an ethoxysilane.[42-45] Therefore, as ethoxysilanes hydrolyze slower than methoxysilanes, they will form more cohesive monolayers on the surface. In our work, AHAP3 is a methoxysilane and AUTES is an ethoxysilane. This explains why AHAP3/NO on the surface has a lower NO payload when on the surface compared with AUTES/NO, despite the situation being reversed in solution phase (Figure S1).

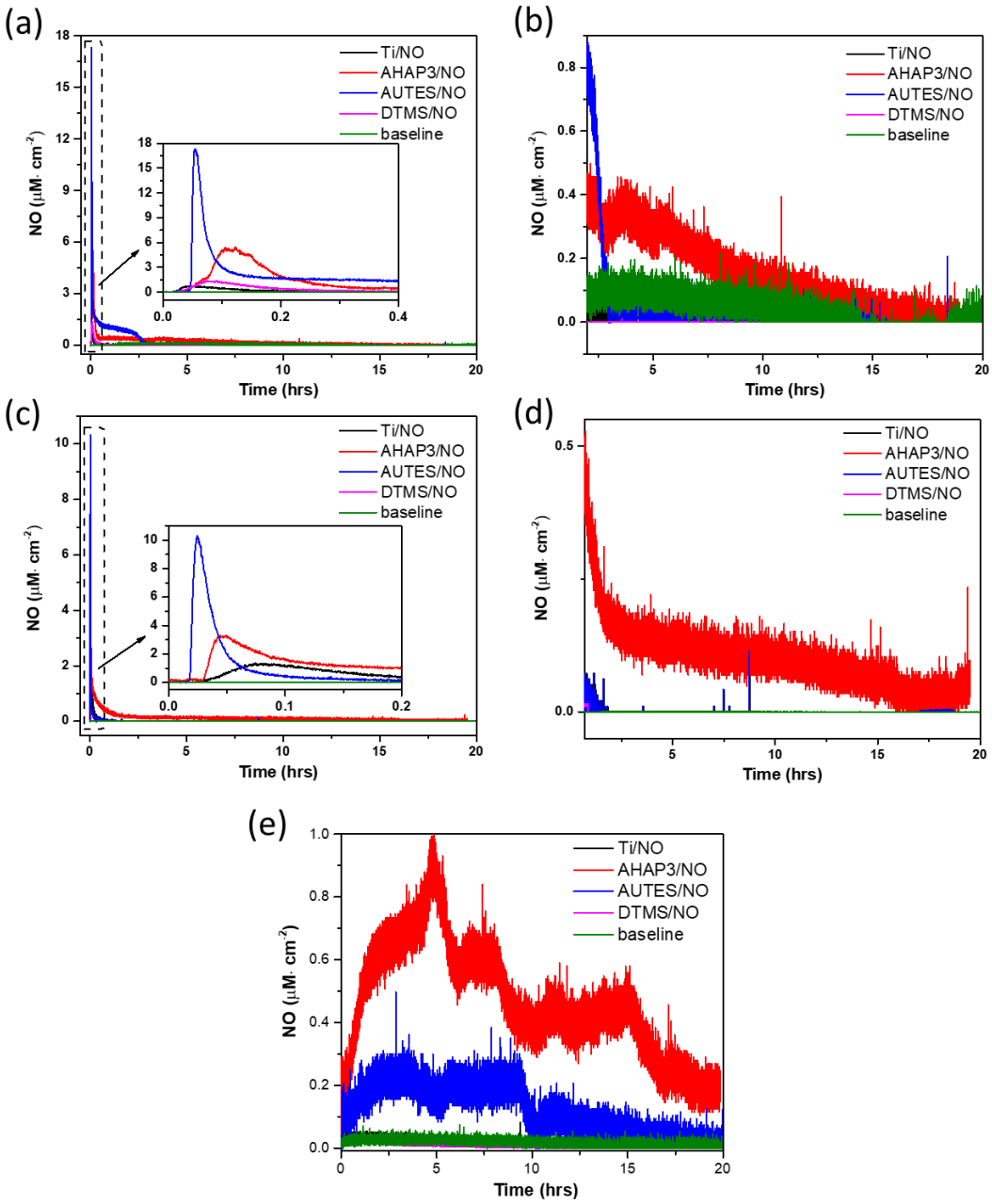

Figure 5. Chemiluminescence NO release profiles of (a) overall 20 hrs and the insert is rescaling of the first 0.4 hr at pH 4, (b) rescale detailing over 20 hrs at pH 4, (c) overall 20 hrs and the insert is rescaling of the first 0.2 hr at pH 7.4, (d) rescale detailing over 20 hrs at pH 7.4 and (e) overall 20 hrs at pH = 8.5 buffers at room temperature. The inserts have the same scaling units of the axis as the overall pictures.

Table 3. NO release properties for diazeniumdiolate-functionalized surfaces prepared by using silane with different amine groups in pH 4, 7.4 and 8.5

	Silane precursor	Number of amine		t[NO] (μM)	t[NO] (μM·cm^{-2})	$t_{1/2}$ (min)	$[NO]_m$ (μM·s^{-1}·cm^{-2})	t_m (min)	t_d (h)
		primary	secondary						
pH 4	AHAP3	1	1	1005.4	3122.4	34.2	5.6	7.4	18.1
	AUTES	1	0	1883.6	5849.7	52.8	17.4	3.2	3.2
	DTMS	0	0	231.1	717.7	8.0	1.3	4.5	0.8
pH 7.4	AHAP3	1	1	676.8	2101.9	16.3	3.1	2.7	16.5
	AUTES	1	0	476.2	1478.9	2.4	10.2	1.5	1.5
	DTMS	0	0	26.0	80.7	0.2	0.3	2.1	0.7
pH 8.5	AHAP3	1	1	330.5	1026.4	183.9	0.9	5.6	20+
	AUTES	1	0	133.7	415.2	159.8	0.3	5.3	10
	DTMS	0	0	-	-	-	-	-	-

3.7 Antimicrobial Analysis. A Gram-positive *S. aureus*, and Gram-negative *P. aeruginosa*, two relevant pathogens for orthopedic infections,[46] were selected to measure the antimicrobial efficacy of NO releasing samples. The SEM micrographs of *S. aureus* and *P. aeruginosa* cultured for 6 hrs on Ti, AHAP3, AUTES and DTMS samples with/without NO release are shown in Figure 6. Bacterial clusters and biofilms can clearly be observed on pristine Ti (as shown in Figure 6a (i)), and all non-NO releasing silanized surfaces (AHAP3, AUTES, and DTMS, Figures 6b-d (i) respectively) demonstrating that these surfaces do not exhibit antimicrobial activity. Tethering of the diazeniumdiolate to the aminosilanized surfaces AHAP3/NO (Figure 6b (ii, iv)) and AUTES/NO (Figure 6c (ii, iv)) demonstrate a reduction in the *S. aureus* and *P. aeruginosa* adhered to the surface, in comparison to Ti/NO (Figure 6a (ii, iv) and DTMS/NO (Figure 6d (ii,iv)). This is in agreement with the results presented in Figure 5, which demonstrates that the surfaces that release the highest payload of NO exhibit the most antimicrobial activity.

The prevention of biofilm formation on all surfaces at 6 and 24 hrs was determined by using a biofilm CFU assay and the results are presented in Figure 6e for *S. aureus*. The AHAP3/NO surface showed a reduction in the number of adhered *S. aureus* from 0.8×10^8 CFU/ml to $\sim10^6$ CFU/ml at 6 hrs which corresponds to a 1.5 log reduction (Figure 6e). Likewise, the AUTES/NO surface showed a reduction in the number of adhered *S. aureus* from 4.1×10^7 CFU/ml to $\sim10^6$ CFU/ml at 6 hrs which corresponds to a 0.8 log reduction (Figure 6e). At 24 hrs, the reduction in the adhered bacteria is approx. 1.5 log for AHAP3 to AHAP3/NO and 0.8 log for AUTES to AUTES/NO. This difference in antimicrobial activity is in agreement with the results presented in Table 3 which show that the AHAP3/NO surface has a higher payload of NO at pH 7.4 (676.8 μM) vs AUTES/NO (476.2 μM). The surface of Ti/NO and DTMS/NO did not show any reduction in the adhered bacteria. A salient point here is that the NO release profiles were carried out in 5 mL of measurement buffer, whilst, the antimicrobial experiments were carried out in 500 μL of broth. Hence the bacteria in these experiments are exposed to 10x the payload observed in the NO release profiles and within the reported range need for antimicrobial activity by Friedman and coworkers[23].

The prevention of biofilm formation on all surfaces at 6 and 24 hrs was determined by using a biofilm CFU assay and the results are presented in Figure 6f for *P. aeruginosa*. The AHAP3/NO surface showed a reduction in the number of adhered *P. aeruginosa* from $\sim10^5$ CFU / ml to 1.6×10^4 CFU / ml at 6 hrs which corresponds to a 0.8 log reduction (Figure 6f). Likewise, the AUTES/NO surface showed a reduction in the number of adhered *P. aeruginosa* from 1.6×10^5 CFU / ml to 3×10^4 CFU / ml at 6 hrs which corresponds to a 0.8 log reduction (Figure 6f). At 24 hrs, the reduction in the adhered bacteria is approx. 0.3 log for AHAP3 to AHAP3/NO and there was no significant reduction for AUTES to AUTES/NO. This difference in antimicrobial activity is in agreement with the results presented in Table 3 which show that the AHAP3/NO surface has a higher payload of NO at pH 7.4 (676.8 μM) vs

AUTES/NO (476.2 μM). The surface of Ti/NO and DTMS/NO did not show any reduction in the adhered bacteria. As mentioned above, as the antimicrobial experiments are carried out in only 500 μl of broth, the bacteria are exposed to 10x the payload observed in the NO release profiles and within the reported range need for antimicrobial activity by Friedman and coworkers[23].

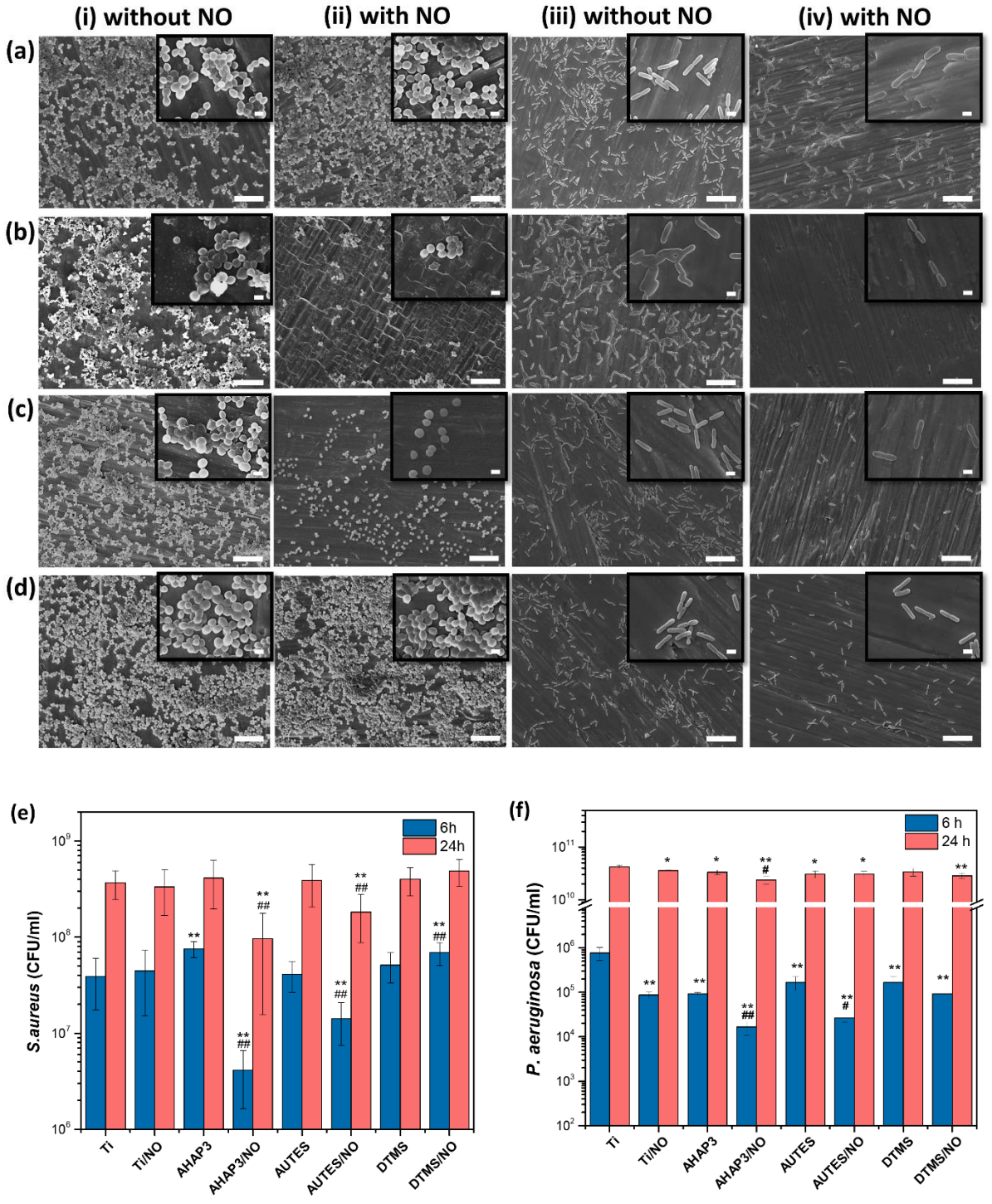

Figure 6. SEM images of (a(i) to d(ii)) *S. aureus* and (a(iii) to d(iv)) *P. aeruginosa* after 6hrs growth on a(i and iii) Ti and (ii and iv)Ti/NO, b(i and iii) AHAP3 and (ii and iv)AHAP3/NO, c(i and iii) AUTES and (ii and iv)AUTES/NO, d(i and iii) DTMS and (ii and iv)DTMS/NO. Inserts in a-d are enlargements of the figures. The scale bar represents 10 µm and 1 µm in insets. (e) *S. aureus* and (f) *P. aeruginosa* colonies formation on the surfaces after 6 hrs and

24 hrs incubation. * $p < 0.05$ and ** $p < 0.01$ from control, and # $p < 0.05$ and ## $p < 0.01$ from corresponding silane.

3.8 Cell Morphology. The morphology of human primary osteoblasts was studied on the various surfaces at 7 days post seeding using confocal laser scanning microscopy (Figure 7). As expected, the osteoblasts present on the control surfaces (pristine Ti (Figure 7a(i)) and DTMS (Figure 7d(i)) were well spread with a high contact area, a complex network of actin fibers and displayed characteristic cobblestone morphology associated with adherent functional osteoblasts. NO treatment of the control surfaces (pristine Ti (Figure 7a(ii)) and DTMS (Figure 7d(ii)) did not affect the morphology of the cells. On the AHAP3 (Figure 7b(i)) and the AUTES (Figure 7c(i)), the osteoblasts had a shrunken morphology, poor actin cytoskeletal formation and there were fewer cells. In direct comparison, qualitative analysis of the cell response to the AHAP3/NO and AUTES/NO surfaces revealed a more positive expression in terms of cell response. Qualitative analysis of these surfaces demonstrated that when cells were cultured in contact with AHAP3/NO (Figure 7 bii) cells were well adhered and spread with a distinctive formation of stress fibers through the body of the cells. Cells cultured in contact with AUTES/NO (Figure 7cii) demonstrated an elevated level of cell adhesion and actin formation compared to AHAP3 surfaces, and even showed formation of the characteristic cobblestone morphology that is associated with well adhered functional osteoblasts and was also apparent on the control surfaces.

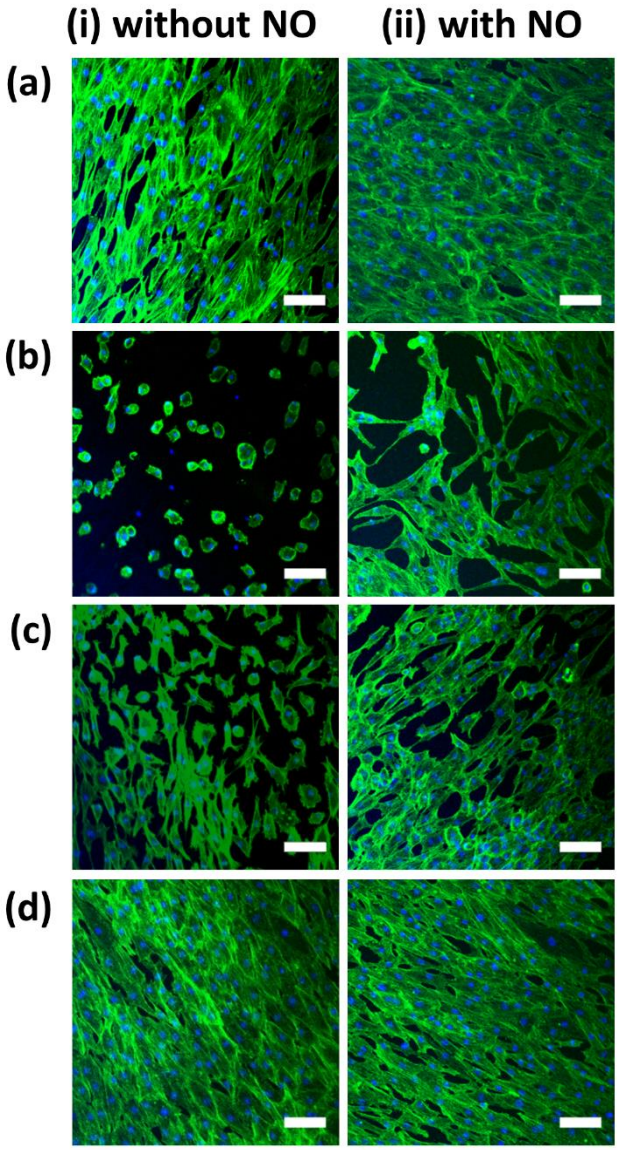

Figure 7. Fluorescence images of human osteoblasts spreading on a(i) Ti and (ii)Ti/NO, b(i) AHAP3 and (ii) AHAP3/NO, c(i) AUTES and (ii) AUTES/NO, d(i) DTMS and (ii) DTMS/NO after 7 days incubation. Representative images, n = 6 per group. Scale bar: 100 μm, F-actin (green) and nucleus (blue).

4. CONCLUSION

The prevention of bacterial adhesion and biofilm formation whilst promoting osteointegration remains a significant medical challenge. We have developed an efficient NO-releasing coating on Ti surfaces. A key focus of this study was to understand mechanistically how aminosilanes tether to the surface and how the nature of the aminosilane precursor affects the resultant NO releasing properties in terms of payload and release kinetics, whilst acting as an initiator for adherence and function of osteoblast cells. The ability of the variously modified surfaces to prevent biofilm formation was evaluated, with both the AHAP3/NO and AUTES/NO surfaces displaying similar antimicrobial efficacy despite having differing inherent NO loading capabilities. Of particular interest is that both AHAP3/NO and AUTES/NO surfaces were capable of prevention of biofilm formation while not displaying cytotoxicity towards human primary osteoblast cells. Experiments are currently underway to evaluate the antimicrobial and osteogenic properties of these surfaces in a bacterial and mammalian co-culture model. Furthermore, macromolecular coatings that are capable of higher NO payloads that result in higher antimicrobial activity are also the subject of ongoing investigation.

ASSOCIATED CONTENT

Supporting Information. This material is available free of charge via the Internet at http://pubs.acs.org. Supplementary data including Table S1 and Figures S1

AUTHOR INFORMATION

Corresponding Author

* r.dsa@liverpool.ac.uk.

ORCID

Man Li: 0000-0002-1210-2667
Jenny Aveyard: 0000-0001-6891-5133
Judith Curran: 0000-0003-2985-3173
Fiona McBride: 0000-0003-2985-3173
Raechelle A. D'Sa: 0000-0003-2651-8783

Notes

The authors declare no competing financial interest.

ACKNOWLEDGMENT

This research was supported by the Engineering and Physical Sciences Institute (EP/M027325/1). M. Li is grateful to the China Scholarship Council for financial support.

REFERENCES

(1) Le Guéhennec, L.; Soueidan, A.; Layrolle, P.; Amouriq, Y. Surface Treatments of Titanium Dental Implants for Rapid Osseointegration. *Dent. Mater.* **2007,** *23*, 844-854.
(2) Salou, L.; Hoornaert, A.; Louarn, G.; Layrolle, P. Enhanced Osseointegration of Titanium Implants with Nanostructured Surfaces: an Experimental Study in Rabbits. *Acta Biomater.* **2015,** *11*, 494-502.
(3) Albrektsson, T.; Brånemark, P. I.; Hansson, H. A.; Lindström, J. Osseointegrated Titanium Implants: Requirements for Ensuring a Long-Lasting, Direct Bone-to-Implant Anchorage in Man. *Acta Orthop. Scand.* **1981,** *52*, 155-170.
(4) Bozic, K. J.; Kurtz, S. M.; Lau, E.; Ong, K.; Chiu, V.; Vail, T. P.; Rubash, H. E.; Berry, D. J. The Epidemiology of Revision Total Knee Arthroplasty in the United States. *Clin. Orthop. Relat. Res.* **2010,** *468*, 45-51.
(5) Bozic, K. J.; Kurtz, S. M.; Lau, E.; Ong, K.; Vail, T. P.; Berry, D. J. The Epidemiology of Revision Total Hip Arthroplasty in the United States. *J. Bone Jt. Surg. Am.* **2009,** *91*, 128-133.
(6) Flemming, H. C.; Wingender, J.; Szewzyk, U.; Steinberg, P.; Rice, S. A.; Kjelleberg, S. Biofilms: an Emergent Form of Bacterial Life. *Nat. Rev. Microbiol.* **2016,** *14*, 563.
(7) Penesyan, A.; Gillings, M.; Paulsen, I. T. Antibiotic Discovery: Combatting Bacterial Resistance in Cells and in Biofilm Communities. *Molecules* **2015,** *20*, 5286-5298.
(8) Arciola, C. R.; Campoccia, D.; Speziale, P.; Montanaro, L.; Costerton, J. W. Biofilm Formation in Staphylococcus Implant Infections. A Review of Molecular Mechanisms and Implications for Biofilm-Resistant Materials. *Biomaterials* **2012,** *33*, 5967-5982.
(9) Zaat, S.; Broekhuizen, C.; Riool, M. Host Tissue as a Niche for Biomaterial-Associated Infection. *Future Microbiol.* **2010,** *5*, 1149-1151.
(10) Campoccia, D.; Montanaro, L.; Arciola, C. R. The Significance of Infection Related to Orthopedic Devices and Issues of Antibiotic Resistance. *Biomaterials* **2006,** *27*, 2331-2339.
(11) Hsieh, P. H.; Lee, M. S.; Hsu, K. Y.; Chang, Y. H.; Shih, H. N.; Ueng, S. W. Gram-Negative Prosthetic Joint Infections: Risk Factors and Outcome of Treatment. *Clin. Infect. Dis.* **2009,** *49*, 1036-1043.
(12) Green, S.; Ripley, M. Chronic Osteomyelitis in Pin Tracks. *J. Bone Joint Surg. Am.* **1984,** *66*, 1092-1098.
(13) Parameswaran, A. D.; Roberts, C. S.; Seligson, D.; Voor, M. Pin Tract Infection with Contemporary External Fixation: How Much of a Problem? *J. Orthop. Trauma* **2003,** *17*, 503-507.
(14) Feng, Q. L.; Wu, J.; Chen, G.; Cui, F.; Kim, T.; Kim, J. A Mechanistic Study of the Antibacterial Effect of Silver Ions on Escherichia Coli and Staphylococcus Aureus. *J. Biomed. Mater. Res.* **2000,** *52*, 662-668.
(15) Xu, Z.; Li, M.; Li, X.; Liu, X.; Ma, F.; Wu, S.; Yeung, K.; Han, Y.; Chu, P. K. Antibacterial Activity of Silver Doped Titanate Nanowires on Ti Implants. *ACS Appl. Mater. Inter.* **2016,** *8*, 16584-16594.
(16) Zhou, Z. H.; Zhang, Y.; Hu, Y. F.; Wahl, L. M.; Cisar, J. O.; Notkins, A. L. The Broad Antibacterial Activity of the Natural Antibody Repertoire is Due to Polyreactive Antibodies. *Cell Host Microbe* **2007,** *1*, 51-61.

(17) Glinel, K.; Jonas, A. M.; Jouenne, T.; Leprince, J.; Galas, L.; Huck, W. T. Antibacterial and Antifouling Polymer Brushes Incorporating Antimicrobial Peptide. *Bioconjugate Chem.* **2008,** *20*, 71-77.
(18) Kazemzadeh-Narbat, M.; Noordin, S.; Masri, B. A.; Garbuz, D. S.; Duncan, C. P.; Hancock, R. E.; Wang, R. Drug Release and Bone Growth Studies of Antimicrobial Peptide-Loaded Calcium Phosphate Coating on Titanium. *J. Biomed. Mater. Res. B* **2012,** *100*, 1344-1352.
(19) Nablo, B. J.; Rothrock, A. R.; Schoenfisch, M. H. Nitric Oxide-Releasing Sol–Gels as Antibacterial Coatings for Orthopedic Implants. *Biomaterials* **2005,** *26*, 917-924.
(20) Aveyard, J. L.; Deller, R. C.; Lace, R.; Williams, R. L.; Kaye, S. B.; Kolegraff, K. N.; Curran, J.; D'Sa, R. A. Antimicrobial Nitric Oxide Releasing Contact Lens Gels for the Treatment of Microbial Keratitis. *ACS Appl. Mater. Inter.* **2019,** *11*, 37491-37501.
(21) Barraud, N.; J Kelso, M.; A Rice, S.; Kjelleberg, S. Nitric Oxide: A Key Mediator of Biofilm Dispersal with Applications in Infectious Diseases. *Curr. Pharm. Des.* **2015,** *21*, 31-42.
(22) Barraud, N.; Storey, M. V.; Moore, Z. P.; Webb, J. S.; Rice, S. A.; Kjelleberg, S. Nitric Oxide-Mediated Dispersal in Single- and Multi- Species Biofilms of Clinically and Industrially Relevant Microorganisms. *Microb. Biotechnol.* **2009,** *2*, 370-378.
(23) Schairer, D. O.; Chouake, J. S.; Nosanchuk, J. D.; Friedman, A. J. The Potential of Nitric Oxide Releasing Therapies as Antimicrobial Agents. *Virulence* **2012,** *3*, 271-279.
(24) Nurhasni, H.; Cao, J.; Choi, M.; Kim, I.; Lee, B. L.; Jung, Y.; Yoo, J. W. Nitric Oxide-Releasing Poly (Lactic-co-Glycolic Acid)-Polyethylenimine Nanoparticles for Prolonged Nitric Oxide Release, Antibacterial Efficacy, and in Vivo Wound Healing Activity. *Int. J. Nanomed.* **2015,** *10*, 3065-3080.
(25) Hetrick, E. M.; Shin, J. H.; Stasko, N. A.; Johnson, C. B.; Wespe, D. A.; Holmuhamedov, E.; Schoenfisch, M. H. Bactericidal Efficacy of Nitric Oxide-Releasing Silica Nanoparticles. *Acs Nano* **2008,** *2*, 235-246.
(26) Yang, L.; Feura, E. S.; Ahonen, M. J. R.; Schoenfisch, M. H. Nitric Oxide–Releasing Macromolecular Scaffolds for Antibacterial Applications. *Adv. Healthc. Mater.* **2018**, *7*, 1800155.
(27) Keefer, L. K. Fifty Years of Diazeniumdiolate Research. From Laboratory Curiosity to Broad-Spectrum Biomedical Advances. *ACS Chem. Bio.* **2011,** *6*, 1147-1155.
(28) Wang, P. G.; Xian, M.; Tang, X.; Wu, X.; Wen, Z.; Cai, T.; Janczuk, A. J. Nitric Oxide Donors: Chemical Activities and Biological Applications. *Chem. Rev.* **2002,** *102*, 1091-1134.
(29) Keefer, L. K.; Nims, R. W.; Davies, K. M.; Wink, D. A. "NONOates"(1-Substituted Diazen-1-ium-1, 2-diolates) as Nitric Oxide Donors: Convenient Nitric Oxide Dosage Forms. *Methods Enzymol.* **1996,** *268*, 281-293.
(30) Ignarro, L. J.; Napoli, C.; Loscalzo, J. Nitric Oxide Donors and Cardiovascular Agents Modulating the Bioactivity of Nitric Oxide: an Overview. *Circ. Res.* **2002,** *90*, 21-28.
(31) Bharadwaj, G.; Benini, P. G. Z.; Basudhar, D.; Ramos-Colon, C. N.; Johnson, G. M.; Larriva, M. M.; Keefer, L. K.; Andrei, D.; Miranda, K. M. Analysis of the HNO and NO Donating Properties of Alicyclic Amine Diazeniumdiolates. *Nitric Oxide* **2014,** *42*, 70-78.
(32) Miranda, K. M.; Katori, T.; Torres De Holding, C. L.; Thomas, L.; Ridnour, L. A.; McLendon, W. J.; Cologna, S. M.; Dutton, A. S.; Champion, H. C.; Mancardi, D. Comparison of the NO and HNO Donating Properties of Diazeniumdiolates: Primary Amine Adducts Release HNO in vivo. *J. Med. Chem.* **2005,** *48*, 8220-8228.
(33) Salmon, D. J.; Torres de Holding, C. L.; Thomas, L.; Peterson, K. V.; Goodman, G. P.; Saavedra, J. E.; Srinivasan, A.; Davies, K. M.; Keefer, L. K.; Miranda, K. M. HNO and NO Release from a Primary Amine-Based Diazeniumdiolate as a Function of pH. *Inorg. Chem.* **2011,** *50*, 3262-3270.

(34) Ho, K. K.; Ozcelik, B.; Willcox, M. D.; Thissen, H.; Kumar, N. Facile Solvent-Free Fabrication of Nitric Oxide (NO)-Releasing Coatings for Prevention of Biofilm Formation. *Chem. Comm.* **2017,** *53*, 6488-6491.
(35) Chen, R.; Hunt, J. A.; Fawcett, S.; D'sa, R.; Akhtar, R.; Curran, J. M. The Optimization and Production of Stable Homogeneous Amine Enriched Surfaces with Characterized Nanotopographical Properties for Enhanced Osteoinduction of Mesenchymal Stem Cells. *J. Biomed. Mater. Res. A* **2018,** *106*, 1862-1877.
(36) Curran, J. M.; Chen, R.; Hunt, J. A. The Guidance of Human Mesenchymal Stem Cell Differentiation in vitro by Controlled Modifications to the Cell Substrate. *Biomaterials* **2006,** *27*, 4783-4793.
(37) Drago, R. S.; Karstetter, B. R. The Reaction of Nitrogen(II) Oxide with Various Primary and Secondary Amines. *J. Am. Chem. Soc.* **1961,** *83*, 1819-1822.
(38) Fleming, G.; Aveyard, J.; Fothergill, J.; McBride, F.; Raval, R.; D'Sa, R. Nitric Oxide Releasing Polymeric Coatings for the Prevention of Biofilm Formation. *Polymers* **2017,** *9*, 601.
(39) Miles, A. A.; Misra, S.; Irwin, J. The Estimation of the Bactericidal Power of the Blood. *Epidemiol. Infect.* **1938,** *38*, 732-749.
(40) Maragos, C. M.; Morley, D.; Wink, D. A.; Dunams, T. M.; Saavedra, J. E.; Hoffman, A.; Bove, A. A.; Isaac, L.; Hrabie, J. A.; Keefer, L. K. Complexes of ·NO with Nucleophiles as Agents for the Controlled Biological Release of Nitric Oxide. Vasorelaxant Effects. *J. Med. Chem.* **1991,** *34*, 3242-3247.
(41) Ragsdale, R. O.; Karstetter, B. R.; Drago, R. S. Decomposition of the Adducts of Diethylamine and Isopropylamine with Nitrogen (II) Oxide. *Inorg. Chem.* **1965,** *4*, 420-422.
(42) Arkles, B.; Steinmetz, J.; Zazyczny, J.; Mehta, P. Factors Contributing to the Stability of Alkoxysilanes in Aqueous Solution. *J. Adhes. Sci. Technol.* **1992,** *6*, 193-206.
(43) Zhu, M.; Lerum, M. Z.; Chen, W. How to Prepare Reproducible, Homogeneous, and Hydrolytically Stable Aminosilane-Derived Layers on Silica. *Langmuir* **2011,** *28*, 416-423.
(44) Asenath Smith, E.; Chen, W. How to Prevent the Loss of Surface Functionality Derived from Aminosilanes. *Langmuir* **2008,** *24*, 12405-12409.
(45) Zhang, F.; Sautter, K.; Larsen, A. M.; Findley, D. A.; Davis, R. C.; Samha, H.; Linford, M. R. Chemical Vapor Deposition of Three Aminosilanes on Silicon Dioxide: Surface Characterization, Stability, Effects of Silane Concentration, and Cyanine Dye Adsorption. *Langmuir* **2010,** *26*, 14648-14654.
(46) Costerton, J. W.; Stewart, P. S.; Greenberg, E. P. Bacterial Biofilms: a Common Cause of Persistent Infections. *Science* **1999,** *284*, 1318-1322.

Table of Contents Graphic